Selective Photocatalytic Reduction of CO<inf>2</inf>-to-CO in Water using a Polymeric Carbon Nitride Quantum Dot/Fe-Porphyrin Hybrid

ChemCatChem

Research Article
doi.org/10.1002/cctc.202200897

Chemistry Europe
European Chemical Societies Publishing

www.chemcatchem.org

Special Collection

Selective Photocatalytic Reduction of CO_2-to-CO in Water using a Polymeric Carbon Nitride Quantum Dot/Fe-Porphyrin Hybrid Assembly

Liam Mistry,[a] Long Le-Quang,[a] Gerard Masdeu,[a] Wilma Björkman,[a] Hanna Härelind,[a] and Maria Abrahamsson*[a]

Visible light-driven conversion of CO_2 into more value-added products is a promising technology not only for diminution of CO_2 emission but also for solar energy storage in the form of chemical energy. However, photocatalytic materials that can efficiently and selectively reduce CO_2-to-CO in a fully aqueous solution typically involve precious metals that limit their suitability for large scale applications. Herein, a novel photocatalytic assembly is reported, consisting of polymeric carbon nitride quantum dots (CNQDs) as the visible light absorber and a Fe-porphyrin complex (Fe-*p*-TMA) as the catalyst for CO_2-to-CO conversion. Both components were carefully selected to allow for excellent solubility in water as well as improved electronic communication through complementary electrostatic and π-π interactions. This CNQD·[Fe-*p*-TMA] hybrid assembly, at the optimized molar ratio, can produce CO with a turnover number (TON) exceeding 10^5 and selectivity ~96% after 10 hours of visible light irradiation (400–700 nm). It is postulated that the enhanced CO_2-to-CO transformation performance is due to the convenience of a more direct charge transfer (CT) pathway between the CNQDs and [Fe-*p*-TMA] motif.

Introduction

The unceasing rise of atmospheric CO_2 over recent decades has placed a great deal of significance on the conversion of CO_2 into organic fuels or value-added products using environmentally responsible methods. However, the inherent stability of the carbon-oxygen double bonds necessitates the use of either electrochemical or catalytic routes to overcome the thermodynamic barrier ($\Delta G^O = 400\ kJ\,mol^{-1}$).[1–4] Therefore, a solar-driven photocatalytic approach to CO_2 reduction (so-called artificial photosynthesis) has become an idyllic concept. Akin to nature, such systems would operate under relatively mild conditions (*i.e.*, at room temperature in water) without additional energy requirements.

Homogeneous catalysts based on non-noble metal complexes have been extensively investigated for their highly tunable electronic and chemical properties.[5] Consequently, they can exhibit very high efficiencies, excellent product selectivity and long-term stability; even at room temperature. Bioinspired iron (Fe), copper (Cu) and cobalt (Co) porphyrin complexes are currently amongst the most promising candidates for use in any real-world future application owed to their low cost and high performance.[6–9] Moreover, by coupling the catalyst to a sensitizer (a visible-light absorber) the performance can be improved by utilizing a wider range of the solar spectrum.[10–13] However, the low photostability of the molecular catalyst brought about by prolonged exposure to UV-light and difficulties associated with recycling are known to be their most prevalent disadvantages.

Iron 5,10,15,20-tetra(4-N,N,N-trimethylanilinium)porphyrin ([Fe-*p*-TMA]·Cl) is, so far, a leading candidate in the search for a sustainable photocatalyst capable of CO_2 reduction within a fully aqueous environment.[7,14] It can be readily synthesized from commercially available components sustainably in a one-pot synthesis. To date, several groups have described [Fe-*p*-TMA] as an efficient, highly selective catalyst for the reduction of CO_2-to-CO. Both electrochemical[7,15,16] and photoassisted[8,17–21] methods have shown high turnover numbers (TON) and selectivity (95% in water at pH 7). The precise mechanism of CO_2-to-CO reduction remains a point of conjecture, however, the overwhelming consensus agree that catalysis occurs at the nucleophilic Fe center forming the Fe–CO_2 adduct, which is then subsequently protonated and reduced leading to the cleavage at one of the two C–O bonds.[22] A suitably positive standard redox potential (E^0 ($Fe^{I/0}$) = −1.50 V *vs.* SCE in DMF) and ability to stabilize intermediate species of the *para*-substituted Fe-porphyrin is thought to be one of its' main virtues.[15]

The addition of a metal-complex photosensitizer, $Ir(ppy)_3$, has been shown to improve the capabilities of [Fe-*p*-TMA]·Cl, exhibiting enhanced CO_2 reduction.[8,19] Visible light irradiation (>420 nm) generates not only CO (72%, $2e^-$ process), but H_2

[a] *Dr. L. Mistry, Dr. L. Le-Quang, Dr. G. Masdeu, W. Björkman, Prof. H. Härelind, Prof. M. Abrahamsson*
Department of Chemistry and Chemical Engineering
Chalmers University of Technology
412 96 Gothenburg (Sweden)
E-mail: abmaria@chalmers.se

Supporting information for this article is available on the WWW under https://doi.org/10.1002/cctc.202200897

This publication is part of a Special Collection on "Photocatalytic Synthesis". Please check the ChemCatChem "https://chemistry-europe.onlinelibrary.wiley.com/doi/toc/10.1002/(ISSN)1867-3899.PhotocatalyticSynthesis"homepage for more articles in the collection.

(10%) and CH_4 (18%, $8e^-$ process). Interestingly, CH_4 was only observed once enough CO had built-up in the system. Despite these encouraging results, the TONs were relatively low in all cases.[8] This approach relies on Brownian motion to facilitate charge transfer events between the $Ir(ppy)_3$ and [Fe-*p*-TMA]. Additional examples of catalytic assemblies and performance parameters can be found in the supporting information, Table S2.

We hypothesize that low catalytic turnover could be overcome by improving the electronic communication between the photosensitizer and catalyst. By ensuring direct communication *via* some means of an intermolecular interaction would encourage the chance of successful charge transfer events, overall enhancing the efficiency of electron migration within the sensitizer-catalyst assembly.

Polymeric carbon nitrogen quantum dots (CNQDs) would be an excellent choice of photosensitizer owed to their stability (limited degradation), solubility in polar solvents, tunable band-gap and wide absorption range (< 650 nm).[23,24] Functionalizing CNQDs with ethylenediaminetetraacetic acid (EDTA) generates negatively charged surface sites (–COO^-), which offer ideal tethering points for the four positively charged *para*-trimethylammonium groups (–$N^+(Me)_3$) of [Fe-*p*-TMA] (Figure 1).[25] Interactions would likely be a combination of π-π interactions and attractive Coulombic forces between the triazine/heptazine surface of CNQDs and [Fe-*p*-TMA] motif.

Results and Discussion

The aim of this study was to develop a superior sensitized photocatalytic system for CO_2-to-CO reduction based on the well-established [Fe-*p*-TMA]·Cl molecular catalyst. The hybrid assembly was stimulated using visible light (400–700 nm) under mild reaction conditions (25 °C) in water. Optimization of that assembly and its components will be the focus of this communication.

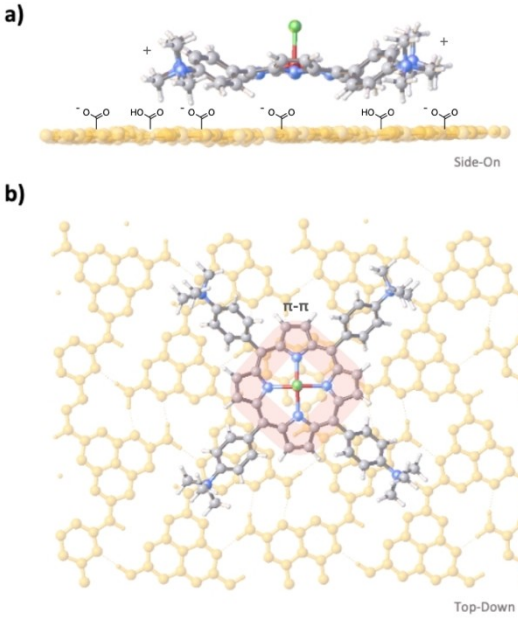

Figure 1. A concept model showing the interactions between [Fe-*p*-TMA]·Cl and tri-*s*-triazine CNQD (pale yellow C/N atoms) surface. Views from a) Side-on and b) Top-down perspective.

The iron porphyrin catalyst, [Fe-*p*-TMA]·Cl (Figure 2a), was prepared using existing literature protocol, by combining 5,10,15,20-Tetrakis(4-trimethylammoniophenyl)-porphyrin tetra(*p*-toluenesulfonate) (TTMAPP) with iron-(II)-bromide ($FeBr_2$) (Figure S5).[15] Characteristic changes in the steady state absorbance (Figure 3 and S6) and electrochemical behavior (CV) confirmed the formation of [Fe-*p*-TMA] stabilized by chlorine counter ions; [Fe-*p*-TMA]·Cl. Bubbling CO_2 through the solution induced a 21 nm hypsochromic blue-shift of the Soret band due to an axial ligand exchange forming the Fe-CO_2 adduct (Figure 3 and S6).[26] The standard redox potential for [Fe-*p*-TMA] (E^0 ($Fe^{I/0}$) = −1.53 V and E^0 ($Fe^{II/I}$) = −0.52 *vs.* Fc/Fc^+) measured in DMF ($TBAPF_6$ 0.1 M) under a blanket N_2 atmosphere fell within the expected range (Figure S7).[7,8,15,27]

CNQDs were synthesised following a well-established microwave-assisted protocol found in the literature.[25] Critically, EDTA did not play a role in the carbonization reaction and acted only as a capping agent as confirmed by IR and XRD (Figure S3 and S4). Without EDTA, the reaction was notably slower to form larger aggregates and lacked the characteristic blue luminescence observed. The photophysical properties are described in detail in the SI, but in short, excitation at 410 nm yields blue steady state emission with φ: 3.8% and an average emission lifetime τ_0: 3.90 ns (Figures 2d and S8–S10). The prepared EDTA-capped CNQDs presented a broad absorption (< 650 nm)[28–32] with a calculated optical band gap energy (E_g) of ~2.44 eV (Equation 1); assuming an indirect band gap (Figure 2b and c).[33–37] High resolution transmission electron microscopy (HRTEM) repeatably revealed regular crystalline dots with diameters ranging between 4–10 nm (Figure 2(i), S1 and S2). Lattice fringes readily observed and measured at 2.8 and 3.1 Å; correlating to the [002] and [100] planes of graphitic carbon nitride.[12,23]

The interaction between the sensitizer and catalyst was investigated using both photolysis experiments and Stern Volmer type quenching studies (Figure S11 and S12). Preliminary charge transfer (CT) experiments (Figure 3 and S11) help support a route involving the Fe^{II}–CO_2 adduct that undergoes a photo-driven transition to form Fe^{I} when irradiated with visible light. The Soret band initially shifts from 413 nm (likely a mixed valence state between Fe^{III} and Fe^{II}) to 392 nm when bubbled with CO_2 (Fe^{II}–CO_2). Interestingly, this occurred spontaneously, even when performed in the dark. Visible light irradiation (400–700 nm) of the saturated Fe-CO_2 solution triggered a prompt transformation in the steady state and the observed Soret band red-shifts from 392 to 425 nm (Figure 3b). A fixed isosbestic point at 411 nm suggests no intermediates were formed during the reaction. This process could be rapidly reversed by re-gassing the solution with CO_2, regenerating the peak at 392 nm. We speculate that a kinetically favorable transition back to Fe^{II}-CO_2 begins from Fe(I) state, rather than the exchange of ligands (–CO or –COOH) from an Fe^{II} or Fe^{III} state. Therefore, the

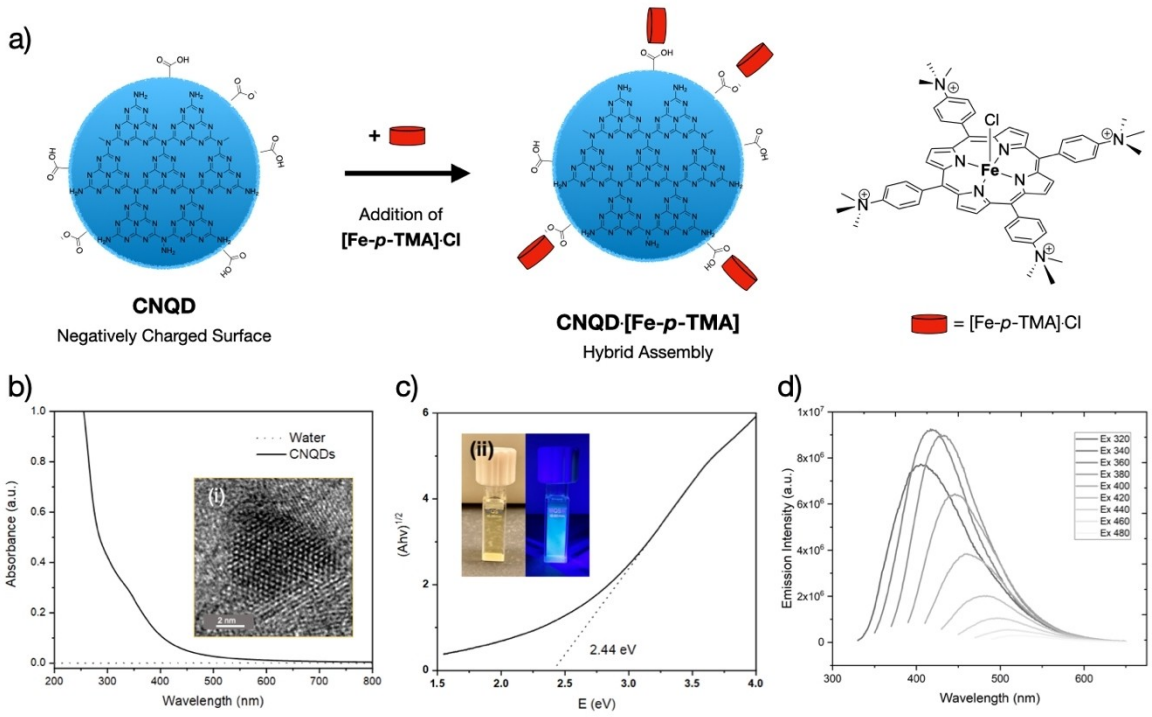

Figure 2. (a) An illustration of the electrostatic interactions between the CNQDs (tri-*s*-triazine or heptazine base pattern) and [Fe-*p*-TMA] motif. (b) The steady state absorbance of CNQDs, (c) Tauc plot and (d) steady state emission (λ_{ex}: 320–480 nm) in water. Inset (i) HRTEM image of a CNQD and (ii) photos demonstrating the luminescence of CNQDs when irradiated with UV-light.

observable transitions bounce between the $Fe^{II} \leftrightarrow Fe^{I}$ states. In the absence of visible light or the sensitizer no such transition occurs. These results further validate the supporting role of the sensitizer in driving the catalytic process.

Steady state emission spectroscopy was used to conduct Stern Volmer type experiments. A quenching rate of $3.3x10^{12}\ M^{-1}s^{-1}$ ($k_q \gg k_{diff}$) was observed following the addition of [Fe-*p*-TMA]. This is interpreted as static quenching due to the inferred pre-association caused by the electrostatic and π-π interactions between the Fe-porphyrin and sensitizer. This is further corroborated by time-resolved emission lifetimes measurements, as the lifetime remained unchanged at 3.90 ns irrespective of Fe-porphyrin concentration (Figure S12e). We hypothesize that these semi-permanent connections facilitate the rapid transfer of electrons between the sensitizer and the catalyst.

CO_2-to-CO catalytic performance

Photocatalytic experiments were carried out in a Pyrex glass photoreactor coupled to a mass spectrometer downstream that continuously monitor gaseous products *in operando* (Figure 4a). The visible light was generated using a Xenon lamp in combination with a UV and an IR filter allowing for the transmission of only visible light (400 - 700 nm, ~55 $mW\,cm^{-2}$ at 405 nm). To remove air from the sample, argon (Ar) gas was purged into the solution at a constant flow rate of 15 mL/min, which was optimal to maintain a stable gas flow while minimizing solvent evaporation at 25 °C. This corresponds to an average gas retention time of 56 seconds in the photoreactor. When measuring catalytic activity, a mixture of CO_2 and Ar (70:30) was continuously bubbled or sparged through the reactor from the base of the solution. The high percentage of CO_2-to-Ar ensured the concentration of CO_2 in solution remained unchanged throughout the reaction. The pH typically dropped from 7.0 to 6.3 over the course of the experiment as the solution became saturated with CO_2. Calibration for CO_2, CO, O_2, H_2 and CH_4 across relevant concentration ranges were conducted before testing (Figure S13). Triethanolamine (TEOA) was added as a sacrificial electron donor (SED); replenishing any positive holes generated within the sensitizer during irradiation.

Initially, the ratio of photosensitizer-to-catalyst was investigated by varying the concentration of [Fe-*p*-TMA] (conc. of CNQDs remained constant at 1.0 g/L) (Figure 4b and Table 1, entries 1, 2[a] and 3). An optimal concentration of 1.0 μM was established (entry 2[a]), yielding ~200 μmol/hr of CO with high selectivity (~96%, ~4% H_2) over 10 hours of irradiation, which translates into TON_{CO} of ~10^5 or TOF_{CO} of ~12 s^{-1}. Increasing the concentration of [Fe-*p*-TMA] to 7.0 μM (entry 3), afforded a 90% drop in CO production giving a TOF of 1.2 s^{-1}. Reducing the catalyst concentration below 1.0 μM (entry 1) also showed heavily diminished CO production. Some studies have shown that the catalyst/photosensitizer ratio has a significant effect on the catalytic performance or CO_2 reduction rate.[20,38–40] This phenomena can be attributed to; (a) less photodegradation of

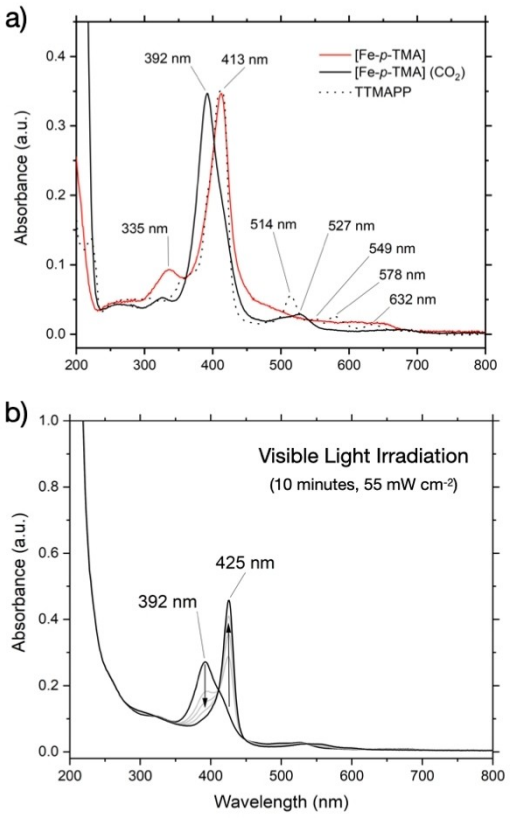

Figure 3. (a) Steady state absorbance of [Fe-*p*-TMA] (red-line), [Fe-*p*-TMA]·CO_2 (black-line) and TTMAPP (dotted-line). (b) Charge transfer (CT) results from [Fe-*p*-TMA]·CNQDs (pre-saturated with CO_2) following illumination with visible-light for 10 minutes.

the catalyst, (b) a higher chance for multiple charge accumulation on the catalyst, (c) each catalyst molecule having greater exposure to CO_2 in solution, or (d) appropriate spatial separation of the Fe motif on the surface of the CNQDs allowing them to function as individual catalytic centers.

In our case, there is little evidence of photodegradation as supported by the sustained production of CO throughout the experiments. Therefore, it is likely a combination of (b), (c) and (d) that dictates our optimized catalyst/sensitizer ratio.

Several control experiments conducted at the optimized concentration ratios of CNQDs·[Fe-*p*-TMA] and TEOA (1.0 g/L, 1.0 μM and 0.1 M respectively, entry $2^{a/b}$, confirmed the photoactive nature of the CO_2-to-CO conversion (Figure 4c, Table 1 and entries 2^b, 4, 5 and 6). CO was not detected (or any other by-products) in the absence of CO_2 or light. Isotope labelling experiments ($^{13}CO_2$, 99%) further validated a catalytic pathway ($^{13}CO_2 \rightarrow {}^{13}CO$) (Figure S14 and Table S3). These results, plus the overall spontaneity of the catalysis helps endorse a photochemical pathway rather than a decomposition route from reactants themselves. No additional reduction products, *i.e.*, CH_3OH, HCOOH, C_2H_5OH, were found in the liquid phase of any of the experiments described. Additionally, no significant quantities of O_2 were generated, indicating that the solvent, water, did not act as an electron donor during the catalytic process to any significant degree.

A solution of only CNQDs (entry 4) delivered CO yields that were down by 84% (TOF = 2.5 s^{-1}) when compared to the optimized hybrid system (entry 2^b, TOF = 15.5 s^{-1}).[41] It is worthwhile to mention that CNQDs have shown catalytic attributes in a heterogenous state (NO decomposition and H_2 evolution from H_2O).[24] In contrast, [Fe-*p*-TMA] alone (entry 5) showed reduced CO_2-to-CO conversion rates and selectivity (TOF = 5.4 s^{-1}, 77%) that could be explained by an inferior photostability. A higher-than-expected rate of CO production could therefore be photodegradation of the catalyst itself, which would otherwise be stabilized by the QDs when irradiated. Photodegradation is a well-established limitation for Fe-base porphyrin complexes. The addition of SEDs allowed the reaction to sustain a higher performance past three hours. Exclusion of TEOA from the mixture resulted in suboptimal CO production over extended time periods (entry 6, TOF = 7.6 s^{-1}). In summary, the combination of each component has been shown to advance the overall catalytic performance and selectivity.

The formation of CH_4 by [Fe-*p*-TMA] has been reported[8] and observed under specific conditions during the course of this study. But, with a focus on CO_2-to-CO conversion these results were not followed-up, yet it's clear from these early results that the conditions play a critical role in both selectivity and catalytic turnover.

There exists ambiguity in the literature regarding the mechanism behind the photo-assisted reduction of CO_2 using a sensitized iron-porphyrin catalyst.[8,17,19,21,22,27] A stepwise reduction of the iron center into a zero-valent state is generally agreed upon as necessary for the formation of the Fe-CO_2 adduct (Fe^{I}-$CO_2^{\bullet -}$ or Fe^{II}–CO_2). Protonation of Fe-CO_2 results in the release of H_2O leaving behind the Fe^{II}-CO intermediate. Photoexcitation of the QD (to QD*) and subsequent donation of a second electron allows for cleavage of CO from the iron-

Table 1. A summary of catalytic performance in water (25 °C) using a sustained CO_2:Ar (70:30) gas flow (15 ml/min). Visible light (400–700 nm) was generated using a Hg–Xe lamp (55 mW cm^{-2}) with the appropriate UV/IR filters. [a] and [b] were prepared separately for their associated data sets.

Entry	Fe-*p*-TMA [μM]	CNQD [g/L]	TEOA [M]	Time [hrs]	CO [μmol h^{-1}]	TON_{CO}	TOF_{CO} [s^{-1}]	Selectivity [%CO]
1	0.0	1.0	0.1	10	60	–	–	74
2^a	1.0	1.0	0.1	10	217	4.3×10^5	12.0	96
2^b	1.0	1.0	0.1	10	279	5.6×10^5	15.5	95
3	7.0	1.0	0.1	10	151	4.3×10^4	1.2	92
4	0.0	1.0	0.0	10	30	–	–	69
5	1.0	0.0	0.0	10	105	1.9×10^5	5.4	77
6	1.0	1.0	0.0	10	136	2.7×10^5	7.6	92

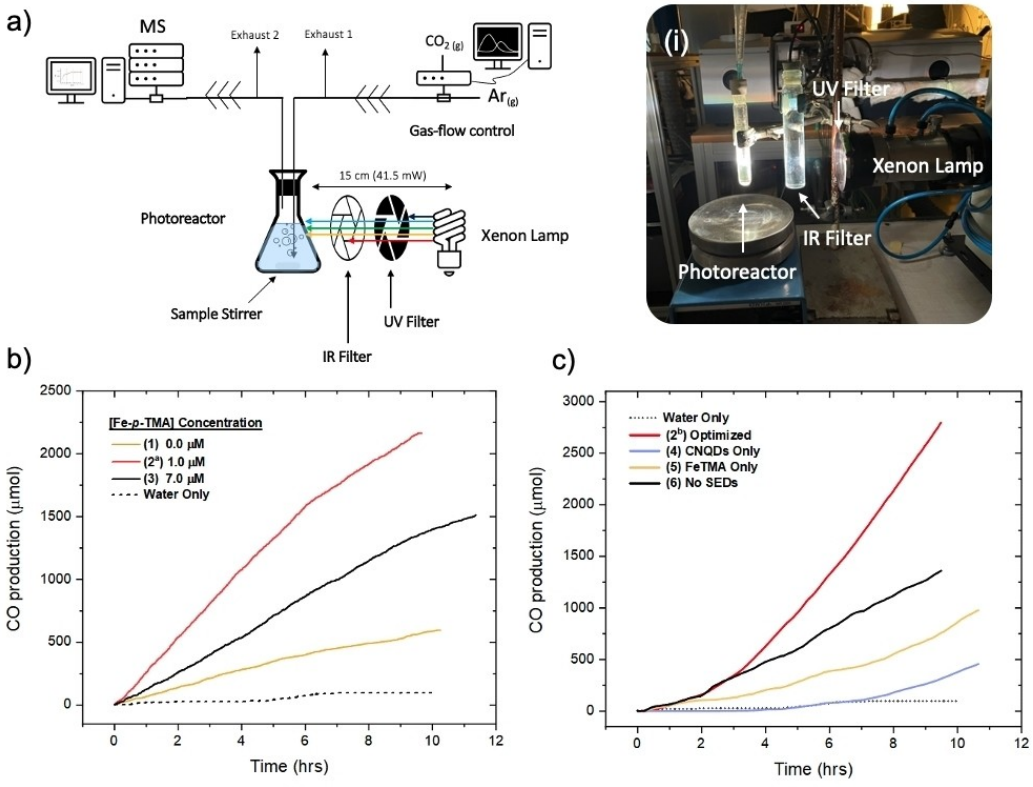

Figure 4. a) A simplistic illustration and (i) photo of the custom photocatalytic set-up used to measure CO_2-to-CO reduction using the hybrid CNQDs·[Fe-p-TMA] system in water at room temperature. Visible light Irradiation involved a Xenon lamp with IR and UV filters (400-700 nm, ~55 mW cm^{-2}). b) and c) show CO production over 10 hours with varying catalyst concentration (0.0, 1.0 and 7.0 μM and 1.0 g/L CNQDs) (b) and with different reaction components (c). These results are summarized in Table 1.

porphyrin. In this work, only the Fe^{II} and Fe^{I} states, but no Fe^{0} state, are observed. Thus, a proposed mechanism based solely on our results would imply a CO formation route *via* a reversible $Fe^{II} \leftrightarrow Fe^{I}$ transformation induced by visible light irradiation of the [Fe-p-TMA]·CNQD assembly in aqueous solution (Figure 5). It should be stressed that the lack of an observed Fe^{0} state does not preclude the existence of such a state. For example, a muted spectroscopic signature relative to the other species present or a very short-lived intermediate state could go undetected in our measurements. A more focused mechanistic study is underway in our laboratories to conclusively identify the acting species in the catalytic cycle.

Conclusion

In summary, we have presented an efficient and selective water-soluble photocatalytic system using: (a) CNQDs as the photosensitizer, (b) [Fe-*p*-TMA] as the catalyst for the reduction of CO_2-to-CO, and (c) visible light as the driving force. Control reactions have confirmed the photocatalytic nature of the conversion. The CNQD:[Fe-*p*-TMA] molar ratio has been optimized, leading to a hybrid catalyst which is able to produce CO with a remarkably high TON of ~10^5 and selectivity of ~96% under ambient conditions (25 °C) using visible light (400–700 nm).

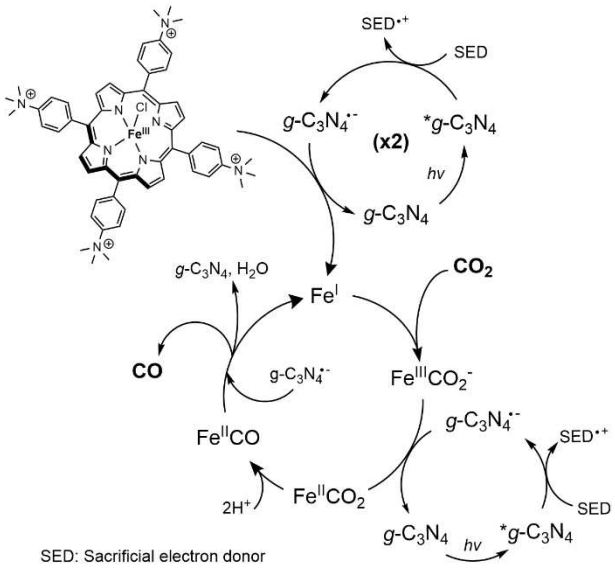

Figure 5. Proposed photocatalytic cycle for the materials used in this work.

The phenomena surrounding power dependent selectivity is an area of great future interest and could potentially allow for

the tuning of products. Further investigations into the mode of interaction and precise mechanistic pathways behind the electron transfers processes could help pave the way towards a novel series of tunable Fe based hybrid photocatalytic systems.

Experimental Section

Materials and chemicals

All reactants were purchased from Sigma Aldrich and used without further purification unless stated otherwise. Methanol (MeOH) and tetrahydrofuran (THF) solvents were dried using 3 Å molecular sieves. Nanopure water was generated using a Milli-Q Advantage A10 system (18.2 MΩ cm resistivity).

CNQD preparation

CNQDs were synthesized according to literature with minor modifications (Figure S1).[25] Guanidine hydrochloride aqueous solution (250 μL, 2.0 mmol, 95.53 g/mol) and EDTA (96 mg, 0.32 mmol, 292.24 g/mol) were dissolved in 20 mL of H_2O. The pH was adjusted to 7.0 ± 0.2 by small additions of concentrated NaOH and/or HCl (1.0 M). Formation of CNQDs was achieved by thermal methods using a household microwave (730 Watt) for approximately four minutes. A brown solid/residue was homogenized in H_2O (40 mL) using a probe ultra-sonicator (97.5 W, 75% Amp, 30 min with 5 sec ON/OFF cycles). Larger particles or flakes within the suspension were separated by centrifugation (8000 rpm, 30 min). The now yellow supernatant solution was collected and concentrated to ~5.5 g/L using rotary evaporation techniques. Further purification was achieved using a dialysis membrane (Pur-A-Lyzer, 3.5 kDa MWCO, 16 hrs) overnight to remove unreacted precursors. CNQDs were retained inside the dialysis membrane. Stock solutions of CNQDs in water (*ca.* 5.5 g/L) were stable for up to four months in the dark.

[Fe-p-TMA]·Cl synthesis

Synthesis of [Fe-*p*-TMA]·Cl followed existing literature protocol (Figure S2).[15] To a round-bottom flask containing dry MeOH (40 mL), 5,10,15,20-tetrakis(4-trimethylammoniophenyl)porphyrin tetra(*p*-toluenesulfonate) (TTMAPP, 38.3 mg, 2.5×10^{-5} mol), anhydrous iron(II) bromide (20 equiv., 5.0×10^{-4} mol, 108.0 mg) and 2,6-lutidine (10 equiv., 2.5×10^{-4} mol, 29 μL) were added. Argon was bubbled through the solution for ~15 min to remove any dissolved O_2. The mixture was refluxed for 7 days under a N_2 atmosphere. MeOH was removed by rotary evaporation and the solid was sonicated in THF before being filtered under vacuum using a glass frit. The remaining solid was washed with DCM, then dissolved in MeOH. The solution was reduced to a volume of around 5 mL using rotary evaporation before ion-exchange. A large volume of THF (*c.a.* 50 mL) was added followed by the dropwise addition of concentrated HCl until a dark precipitate emerged whilst being stirred. The precipitate was isolated using vacuum filtration over a glass frit, then washed with THF and subsequently collected using MeOH. The solid was dried under reduced pressure to yield [Fe-*p*-TMA]·Cl as a dark red powder (24.0 mg, 96%).

Optical band-gap calculations

Determining the optical band-gap energy of CNQDs based on UV-vis spectra was achieved using the Tauc method.[42] Assuming the energy-dependent absorption coefficient α can be expressed by Equation (1):

$$(\alpha \cdot h\nu)^{1/\gamma} = B(h\nu - E_g) \tag{1}$$

Where h is the Planck constant, ν is the photon's frequency, E_g is the optical band-gap energy and B is a constant. The γ factor depends on the nature of the electron transition and is equal to $^1/_2$ or 2 for direct and indirect transition band gap respectively. Here, we assume an indirect band gap semiconductor. The point of *x*-axis intersection to the linear fit of the Tauc plot gives an estimation of the band-gap energy.

Catalytic yield calculations

Photocatalytic reduction of CO_2 was achieved using a custom gas-flow set-up with a continuous flow rate of 15 mL/min (CO_2:Ar (70:30)). A high-pressure 450 W Hg–Xe lamp (Newport) equipped with a 399 nm long-pass filter and a water filter was used to produce visible light. Considering the optical transparency of the Pyrex photoreactor (~80% in the 400–800 nm range), the incident light power density was measured at 55 ± 10 mW cm^{-2} with an Ophir 3 A power/energy sensor. The photoreactor was held 12 cm away from the aperture of the xenon lamp. The gas outlet of the photoreactor was connected to a mass spectrometer (Hiden Analytical, HPR-20 QIC) to analyse gaseous products in real time. Calibrations for gases (CO_2, CO, CH_4, H_2, O_2) and liquids (HCOOH, MeOH) that might be involved in the CO_2 reduction process were periodically performed in a suitable range (*supporting information*).

The molar mass of a gas can be found using the slope derived from %gas calibration plot *versus* MS intensity using Equation (2):

$$V_{gas}(t) = V_{gas}(\text{headspace}) + V_{gas}(\text{flow}) = \%Gas(t) \times V_{dead} + \nu \int_{t_0}^{t} \%gas(t)dt \tag{2}$$

Where, V_{dead} is the headspace (14 mL), ν is the gas flowrate per hour (900 mL/hr = 15 mL/min), time is in hour units.

Selectivity describes the abilities of a catalyst to produce a specific reaction product and is typically reported as molar percentage of total conversion, as shown in Equation (3):

$$selectivity(\%) = 100 \times {}^{n_{prod}}/_{n_{total}} \tag{3}$$

Where n_{prod} is the product of interest (mole) and n_{total} is the sum of total products formed (mole)

Turnover number (TON, Equation (4)) and turnover frequency (TOF, equation (5)) are quantifiers for catalytic performance and reflect the stability of the system and rate of product formation. TON_{CO} represents the overall number of moles of carbon monoxide formed per mole of catalyst. TOF_{CO} is defined as the TON_{CO} per unit of time.

$$TON_{CO} = {}^{n_{CO}}/_{n_{cat}} \tag{4}$$

$$TOF_{CO} = {}^{TON_{CO}}/_{t} \tag{5}$$

Where n_{cat} is the amount of catalyst present in the system (mole) and t is time in seconds.

All other characterization data, original spectra, etc., is provided in the Supporting Information.

Acknowledgements

We gratefully acknowledge Åforsk foundation, Sweden for their financial support. We'd also like to thank Chalmers Materials Analysis Laboratory (CMAL) for their assistance in data collection. A special mention to Stefan Gustafsson for his technical expertise and guidance with all things involving electron microscopy. At the time of publication, Dr Gerard Masdeu is an employee of Astra Zeneca, Sweden.

Conflict of Interest

The authors declare no conflict of interest.

Data Availability Statement

The data that support the findings of this study are available from the corresponding author upon reasonable request.

Keywords: CO_2 reduction · Fe-porphyrin · photocatalysis · polymeric carbon nitride · solar-to-fuels

[1] Y. Ma, X. Wang, Y. Jia, X. Chen, H. Han, C. Li, *Chem. Rev.* **2014**, *114*, 9987–10043.
[2] J. L. White, M. F. Baruch, J. E. Pander, Y. Hu, I. C. Fortmeyer, J. E. Park, T. Zhang, K. Liao, J. Gu, Y. Yan, T. W. Shaw, E. Abelev, A. B. Bocarsly, *Chem. Rev.* **2015**, *115*, 12888–12935.
[3] G. Zhao, X. Huang, X. Wang, X. Wang, *J. Mater. Chem. A* **2017**, *5*, 21625–21649.
[4] M. Aresta, A. Dibenedetto, A. Angelini, *Chem. Rev.* **2014**, *114*, 1709–1742.
[5] K. E. Dalle, J. Warnan, J. J. Leung, B. Reuillard, I. S. Karmel, E. Reisner, *Chem. Rev.* **2019**, *119*, 2752–2875.
[6] Z. Weng, J. Jiang, Y. Wu, Z. Wu, X. Guo, K. L. Materna, W. Liu, V. S. Batista, G. W. Brudvig, H. Wang, *J. Am. Chem. Soc.* **2016**, *138*, 8076–8079.
[7] I. Azcarate, C. Costentin, M. Robert, J. M. Savéant, *J. Am. Chem. Soc.* **2016**, *138*, 16639–16644.
[8] H. Rao, L. C. Schmidt, J. Bonin, M. Robert, *Nature* **2017**, *548*, 74–77.
[9] Z. Weng, Y. Wu, M. Wang, J. Jiang, K. Yang, S. Huo, X. F. Wang, Q. Ma, G. W. Brudvig, V. S. Batista, Y. Liang, Z. Feng, H. Wang, *Nat. Commun.* **2018**, *9*, 1–9.
[10] G. Zhao, H. Pang, G. Liu, P. Li, H. Liu, H. Zhang, L. Shi, J. Ye, *Appl. Catal. B* **2017**, *200*, 141–149.
[11] L. Lin, C. Hou, X. Zhang, Y. Wang, Y. Chen, T. He, *Appl. Catal. B* **2018**, *221*, 312–319.
[12] A. Kumar, P. K. Prajapati, M. S. Aathira, A. Bansiwal, R. Boukherroub, S. L. Jain, *J. Colloid Interface Sci.* **2019**, *543*, 201–213.
[13] J. Liu, H. Shi, Q. Shen, C. Guo, G. Zhao, *Green Chem.* **2017**, *19*, 5900–5910.
[14] J. Bonin, A. Maurin, M. Robert, *Coord. Chem. Rev.* **2017**, *334*, 184–198.
[15] C. Costentin, M. Robert, J. M. Savéant, A. Tatin, *Proc. Natl. Acad. Sci. USA* **2015**, *112*, 6882–6886.
[16] C. Costentin, S. Drouet, M. Robert, J.-M. Savéant, *Science* **2012**, *338*, 90–94.
[17] H. Rao, C. H. Lim, J. Bonin, G. M. Miyake, M. Robert, *J. Am. Chem. Soc.* **2018**, *140*, 17830–17834.
[18] B. Mondal, P. Sen, A. Rana, D. Saha, P. Das, A. Dey, *ACS Catal.* **2019**, *9*, 3895–3899.
[19] J. Bonin, M. Robert, M. Routier, *J. Am. Chem. Soc.* **2014**, *136*, 16768–16771.
[20] H. Rao, J. Bonin, M. Robert, *ChemSusChem* **2017**, *10*, 4447–4450.
[21] H. Rao, J. Bonin, M. Robert, *Chem. Commun.* **2017**, *53*, 2830–2833.
[22] J. Bonin, M. Chaussemier, M. Robert, M. Routier, *ChemCatChem* **2014**, *6*, 3200–3207.
[23] T. S. Miller, A. B. Jorge, T. M. Suter, A. Sella, F. Corà, P. F. McMillan, *Phys. Chem. Chem. Phys.* **2017**, *19*, 15613–15638.
[24] J. Zhu, P. Xiao, H. Li, S. A. C. Carabineiro, *ACS Appl. Mater. Interfaces* **2014**, *6*, 16449–16465.
[25] Y. Tang, Y. Su, N. Yang, L. Zhang, Y. Lv, *Anal. Chem.* **2014**, *86*, 4528–4535.
[26] T. Ohya, M. Sato, *Bull. Chem. Soc. Jpn.* **1996**, *69*, 3201–3205.
[27] S. Lian, M. S. Kodaimati, D. S. Dolzhnikov, R. Calzada, E. A. Weiss, *J. Am. Chem. Soc.* **2017**, *139*, 8931–8938.
[28] G. A. M. Hutton, B. C. M. Martindale, E. Reisner, *Chem. Soc. Rev.* **2017**, *46*, 6111–6123.
[29] Y. P. Sun, B. Zhou, Y. Lin, W. Wang, K. A. S. Fernando, P. Pathak, M. J. Meziani, B. A. Harruff, X. Wang, H. Wang, P. G. Luo, H. Yang, M. E. Kose, B. Chen, L. M. Veca, S. Y. Xie, *J. Am. Chem. Soc.* **2006**, *128*, 7756–7757.
[30] G. E. Lecroy, F. Messina, A. Sciortino, C. E. Bunker, P. Wang, K. A. S. Fernando, Y. P. Sun, *J. Phys. Chem. C* **2017**, *121*, 28180–28186.
[31] Z. Zhou, Y. Zhang, Y. Shen, S. Liu, Y. Zhang, *Chem. Soc. Rev.* **2018**, *47*, 2298–2321.
[32] J. Wen, J. Xie, X. Chen, X. Li, *Appl. Surf. Sci.* **2017**, *391*, 72–123.
[33] Y. Wang, X. Wang, M. Antonietti, *Angew. Chem. Int. Ed.* **2012**, *51*, 68–89; *Angew. Chem.* **2012**, *124*, 70–92.
[34] G. Liao, Y. Gong, L. Zhang, H. Gao, G. J. Yang, B. Fang, *Energy Environ. Sci.* **2019**, *12*, 2080–2147.
[35] W. Tu, Y. Xu, J. Wang, B. Zhang, T. Zhou, S. Yin, S. Wu, C. Li, Y. Huang, Y. Zhou, Z. Zou, J. Robertson, M. Kraft, R. Xu, *ACS Sustainable Chem. Eng.* **2017**, *5*, 7260–7268.
[36] X. Wang, K. Maeda, A. Thomas, K. Takanabe, G. Xin, J. M. Carlsson, K. Domen, M. Antonietti, *Nat. Mater.* **2009**, *8*, 76–80.
[37] R. Godin, Y. Wang, M. A. Zwijnenburg, J. Tang, J. R. Durrant, *J. Am. Chem. Soc.* **2017**, *139*, 5216–5224.
[38] S. Lian, M. S. Kodaimati, E. A. Weiss, *ACS Nano* **2018**, *12*, 568–575.
[39] A. Call, M. Cibian, K. Yamamoto, T. Nakazono, K. Yamauchi, K. Sakai, *ACS Catal.* **2019**, *9*, 4867–4874.
[40] X. Zhang, M. Cibian, A. Call, K. Yamauchi, K. Sakai, *ACS Catal.* **2019**, *9*, 11263–11273.
[41] Y. Wang, X. Bai, H. Qin, F. Wang, Y. Li, X. Li, S. Kang, Y. Zuo, L. Cui, *ACS Appl. Mater. Interfaces* **2016**, *8*, 17212–17219.
[42] P. Makuła, M. Pacia, W. Macyk, *J. Phys. Chem. Lett.* **2018**, *9*, 6814–6817.

Manuscript received: July 15, 2022
Revised manuscript received: October 31, 2022
Accepted manuscript online: November 2, 2022
Version of record online: ■■, ■■■

RESEARCH ARTICLE

Visible light driven catalytic reduction of CO_2 to CO using a well-known iron-porphyrin catalyst electrostatically coupled to functionalized carbon nitride quantum dots. The hybrid assembly has shown excellent sustained performance under relatively mild conditions with high TON and selectivity of approximately 96% in water.

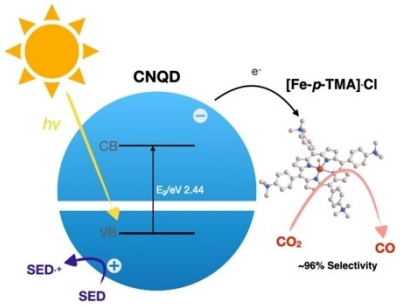

*Dr. L. Mistry, Dr. L. Le-Quang, Dr. G. Masdeu, W. Björkman, Prof. H. Härelind, Prof. M. Abrahamsson**